Modeling of Casting, Welding and Advanced Solidification Processes X, San Destin, FL, May 25-30, 2003
Edited by D. Stefanescu, M. Jolly, J. Warren, and M. Krane
TMS (The Minerals, Metals & Materials Society), 2003, pp. 385-392

THERMO-MECHANICAL FINITE ELEMENT MODEL OF SHELL BEHAVIOR IN CONTINUOUS CASTING OF STEEL

Chunsheng Li and Brian G. Thomas

University of Illinois at Urbana-Champaign,
Department of Mechanical and Industrial Engineering,
1206 West Green Street, Urbana, IL USA, 61801

Abstract

A finite-element model, CON2D, has been developed to simulate temperature, shape, stress, and hot-tear crack development during the continuous casting of steel, both in and below the mold. The stress model features an elastic-viscoplastic creep constitutive equation that accounts for the different responses of the liquid, semi-solid, delta-ferrite, and austenite phases. Temperature and composition-dependent functions are also employed for properties such as thermal linear expansion. A contact algorithm prevents penetration of the shell into the mold wall due to the internal liquid ferrostatic pressure. An efficient two-step algorithm has been developed to integrate these highly non-linear equations. An inelastic strain-based criterion is developed to predict damage leading to hot-tear crack formation, which includes the contribution of liquid flow during feeding of the mushy zone. The model is validated with an analytical solution for temperature and stress in a solidifying plate. It is then applied to predict the maximum casting speed to avoid crack formation due to bulging below the mold during casting of square steel billets.

Introduction

Computational models are important tools to study complex processes such as the continuous casting of steel. They can help to understand how defects form and to optimize casting conditions to maximize quality and productivity at low cost. Several previous researchers have developed two-dimensional (2-D) thermal-mechanical finite element models to study crack formation in continuous cast steel billets [1-4]. One such model, CON2D, has been developed at the University of Illinois over the past decade [5-7]. It has been applied to simulate shell thinning breakouts [5], ideal taper optimization [5], and meniscus distortion [6, 7]. This paper briefly summarizes the features of this model, including a new hot-tearing criterion, and then describes its recent application to predict the maximum casting speed to avoid crack formation due to bulging below the mold during continuous casting of square billets.

Model Description

Heat Transfer and Solidification Model

The model solves a 2-D finite-element discretization of the transient heat conduction equation in a Lagrangian reference frame that moves down the caster with the solidifying steel shell. It features a spatial averaging method by Lemon to handle latent heat evolution [8] and a three-level time-stepping method by Dupont [9].

Stress Model

The equilibrium, constitutive, and strain-displacement equations in this 2-D slice through the shell are solved under a condition of generalized plane strain in the casting direction [5]. The total strain increment, $\{\Delta\varepsilon\}$, is composed of elastic, $\{\Delta\varepsilon_e\}$, thermal, $\{\Delta\varepsilon_{th}\}$, inelastic strain, $\{\Delta\varepsilon_{in}\}$, and flow strain, $\{\Delta\varepsilon_{flow}\}$, components. Thermal strain due to volume changes caused by both temperature differences and phase transformations is calculated from the thermal linear expansion (TLE) of the material, which is based on density measurements.

$$\{\varepsilon_{th}\} = \left(TLE(T) - TLE(T_0)\right)\{1 \quad 1 \quad 0 \quad 1\}^T \quad where \quad TLE(T) = \sqrt[3]{\rho(T_0)/\rho(T)} - 1 \qquad (1)$$

A unified constitutive model is used here to capture the temperature- and strain-rate sensitivity of high temperature steel. The instantaneous equivalent inelastic strain rate ε_{in} is adopted as the scalar state function, which depends on the current equivalent stress, $\bar{\sigma}$, temperature, T, the current equivalent inelastic strain, ε_{in}, which accumulates below the solidus temperature, and carbon content of the steel. When the steel is mainly austenite, (%γ >90%), Model III by Kozlowski [10] was applied. This function matches tensile test measurements of Wray [11] and creep test data of Suzuki [12]. When the steel contains significant amounts of soft delta-ferrite (%δ >10%), a power-law model is used, which matches measurements of Wray above 1400 ^{o}C [6, 13]. Fig. 1 shows the accuracy of the constitutive model predictions compared with stresses measured by Wray [14] at 5% strain at different strain rates and temperatures. This figure also shows the higher strength of austenite, which governs stress development in the solidifying shell. The von-Mises yield surface, with plasticity and normality hypotheses in the Prandtl-Reuss flow rule is applied to model isotropic hardening of these plain carbon steels [15].

A fixed-grid approach is employed which gives no special treatment to liquid elements. To enforce negligible shear stress in the liquid, the following constitutive equation is used to provide a very rapid creep strain rate in every element containing any liquid, (ie., $T > T_{solidus}$).

$$\dot{\bar{\varepsilon}}_{flow} = \begin{cases} 10^8 \left(|\bar{\sigma}| - \sigma_{yield} \right)^5 & |\bar{\sigma}| > \sigma_{yield} \\ 0 & |\bar{\sigma}| \le \sigma_{yield} \end{cases} \quad where \quad \sigma_{yield} = 0.01 MPa \tag{2}$$

The same Prandtl-Reuss relation used for the solid is adopted to expand this scalar strain rate to its multi-dimensional vector. This fixed-grid approach avoids difficulties of adaptive meshing and allows strain to accumulate in the mushy region, which is important for the prediction of hot-tear cracks. As in the real system, the total mass of the liquid domain is not constant: the inelastic strain accumulated in the liquid region represents mass transport due to fluid flow in and out of the domain, so is denoted as "flow strain". Positive flow strain indicates fluid feeding into the simulated region.

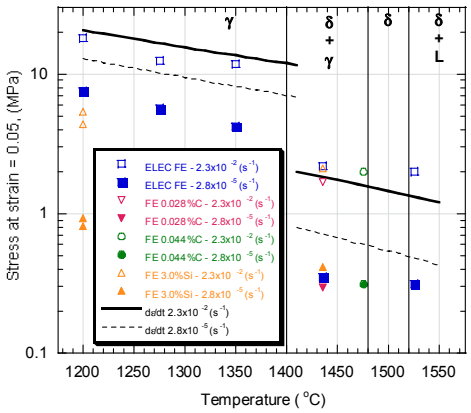

Figure 1: Comparison of predicted and measured stress [14]

Finite Element Implementation. Applying the standard Galerkin's method to the governing equations gives the linear algebraic equations to solve for temperature and then displacement within each time step. The stress model uses 6-node quadratic-displacement triangular elements, which were each divided into four 3-node linear-temperature elements for the heat transfer calculation. The stress calculation involves force vectors due to increments of thermal and inelastic strain, ferrostatic pressure and shell/mold interaction at special internal boundaries, and elastic strain corrections from the previous time step. Ferrostatic pressure from the liquid steel is applied as concentrated force on those nodes whose temperature is just below the solidus. An efficient contact algorithm based on penalty method, developed by Moitra [5], is adopted to prevent shell from penetrating the mold wall, while allowing it shrink freely.

$$[K]\{\Delta u\}^{t+\Delta t} = \left\{\Delta F_{\varepsilon_{th}}\right\}^{t+\Delta t} + \left\{\Delta F_{\varepsilon_{pl}}\right\}^{t+\Delta t} + \left\{F_{fp}\right\}^{t+\Delta t} + \left\{F_{el}\right\}^{t+\Delta t} \tag{3}$$

Integration of the Constitutive Model. The highly strain-rate-dependent constitutive models involved in this solidification problem require a robust numerical integration technique to avoid numerical difficulties. This work applies a "local-global" method that alternates in each time step between implicit time integration of the constitutive equations to accurately estimate the future stress at each Gauss point, followed by standard finite element spatial integration. Specifically, the integration procedure used within each time step is summarized as:

1. Estimate $\{\Delta\hat{\varepsilon}\}$ based on $\{\Delta u\}$ from the previous time step: $\{\Delta\hat{\varepsilon}\} = [B]\{\Delta u\}^t$.
2. Calculate $\left\{\sigma^*\right\}^{t+\Delta t}$, $\bar{\sigma}^*$ and $\left\{\sigma^{*\prime}\right\}^{t+\Delta t}$, needed to define the direction of the stress vector.

$$\left\{\sigma^*\right\}^{t+\Delta t} = [D]^{t+\Delta t}\left(\{\varepsilon\}^t - \{\varepsilon_{th}\}^t - \{\varepsilon_{in}\}^t + \{\Delta\hat{\varepsilon}\} - \dot{\varepsilon}_{th}^{t+\Delta t}\Delta t\{1 \quad 1 \quad 0 \quad 1\}^T\right) \tag{4}$$

3. Solve the following two ordinary differential equations simultaneously for $\bar{\varepsilon}_{in}^{t+\Delta t}$ and $\bar{\hat{\sigma}}^{t+\Delta t}$ at each local Gauss point, using a fully implicit bounded Newton-Raphson integration method from Lush [16]. This method gives the best robustness and efficiency of several alternative approaches evaluated [6]. Function F is either Kozlowski model III for γ, the power law for δ, or flow strain for liquid phase.

$$\bar{\varepsilon}_{in}^{t+\Delta t} = \bar{\varepsilon}_{in}^{t} + F\left(T, \bar{\hat{\sigma}}^{t+\Delta t}, \bar{\varepsilon}_{in}^{t+\Delta t}, \%C\right)\Delta t$$
$$\bar{\hat{\sigma}}^{t+\Delta t} = \bar{\sigma}^{*t+\Delta t} - 3\mu^{t+\Delta t} F\left(T, \bar{\hat{\sigma}}^{t+\Delta t}, \bar{\varepsilon}_{in}^{t+\Delta t}, \%C\right)\Delta t \quad (5)$$

4. Expand this scalar stress estimate into vector form: $\{\hat{\sigma}\}^{t+\Delta t} = \bar{\hat{\sigma}}^{t+\Delta t}\frac{\{\sigma^{*}{}'\}^{t+\Delta t}}{\bar{\sigma}^{*t+\Delta t}} + \frac{1}{3}\sigma_m^{*t+\Delta t}\{\delta\}^T$.

where $\{\sigma^{*}{}'\}^{t+\Delta t} = \{\sigma^{*}\}^{t+\Delta t} - \frac{1}{3}\sigma_m^{*t+\Delta t}\{\delta\}^T$; $\sigma_m^{*t+\Delta t} = \sigma_x^{*t+\Delta t} + \sigma_y^{*t+\Delta t} + \sigma_z^{*t+\Delta t}$; $\{\delta\} = \{1 \quad 1 \quad 0 \quad 1\}$

5. Calculate $\dot{\bar{\varepsilon}}_{in}^{t+\Delta t}$ from $\bar{\hat{\sigma}}^{t+\Delta t}$ and $\bar{\varepsilon}_{in}^{t+\Delta t}$ using F according to the material phase.

6. Expand $\dot{\bar{\varepsilon}}_{in}^{t+\Delta t}$ into a vector $\{\dot{\varepsilon}_{in}\}^{t+\Delta t}$ with the same direction as $\{\hat{\sigma}'\}^{t+\Delta t}$ using Prandtl-Reuss eqs.; Update $\{\varepsilon_{in}\}^{t+\Delta t} = \{\varepsilon_{in}\}^{t} + \{\dot{\varepsilon}_{in}\}^{t+\Delta t}\Delta t$ only for solidified elements.

7. Use classic FEM spatial integration to solve Eq. 3 or $\{\Delta u\}^{t+\Delta t}$ based on $\{\hat{\sigma}\}^{t+\Delta t}$ and $\{\dot{\varepsilon}_{in}\}^{t+\Delta t}$.

8. Finally, find $\{\Delta\varepsilon\}^{t+\Delta t}$ from $\{\Delta u\}^{t+\Delta t}$ and update $\{\varepsilon\}^{t+\Delta t}$ and $\{\sigma\}^{t+\Delta t}$.

Hot-tear Criterion. A simple empirical critical strain function, ε_c, fitted by Won [17] from many measurements, was adopted in this work as a criterion to indicate hot tears (Eq. 6). Hot-tear cracks form if the thick dendrites in the brittle temperature range, ΔT_B [17], prevent the surrounding liquid from compensating the contraction of interdendritic liquid and solid expansion. Cracks are predicted when hot-tear strain, $\varepsilon_{hot\text{-}tear}$, exceeds the critical strain, ε_c.

$$\varepsilon_{hot-tear} \geq \varepsilon_c \quad where \quad \varepsilon_{hot-tear} = \sum_{f_s=0.9}^{f_s=0.99} \Delta\varepsilon_{flow\_hoop} \quad and \quad \varepsilon_c = \frac{0.02821}{\dot{\varepsilon}^{0.3131}\Delta T_B^{\,0.8638}} \quad (6)$$

Hot-tear strain is defined as the flow strain accumulated within the brittle temperature range, calculated during the post-processing phase. The hot-tear strain component chosen for comparison is taken perpendicular to the dendrite growth direction, which is along the "hoop" direction, so named because it is tangential to the surface of the solidifying shell.

Model Validation

An analytical solution of thermal stress in an unconstrained solidifying plate developed by Weiner and Boley [18] is used as a test problem to validate this solidification stress model. The elastic-perfectly-plastic constitutive equation used in this solution was transformed to a numerically challenging rate formulation in Eq. 2 and computed by CON2D.

Table I: Steel Used in Billet Analysis

Steel Composition (wt%)	0.27C, 1.52Mn, 0.34Si, 0.015S, 0.012P
Liquidus Temp. (°C)	1500.72
70% Solid Temp. (°C)	1477.02
90% Solid Temp. (°C)	1459.90
Solidus Temp. (°C)	1411.79

Table II: Simulation Conditions

Billet Section Size (mm×mm)	120×120
Total Mold Length (mm)	800
Meniscus Level (mm)	100
Mesh Size (mm×mm)	0.1×0.1~1.4×1.0
Number of Nodes	7381
Time Step Size (sec.)	0.001 – 0.5
Pouring Temperature (°C)	1540.0

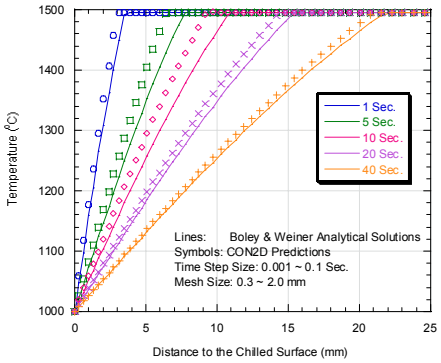

Figure 2: Temperatures through solidifying plate at different times compared with analytical solution

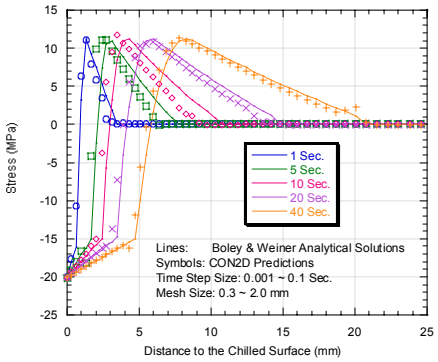

Figure 3: Stresses through solidifying plate at different times compared with analytical solution

Figs. 2 and 3 show the analytical solutions compared with CON2D predictions. The CON2D results match within 2% average error for the same mesh and time step sizes used in the actual 2-D caster simulations – Table II. This demonstrates that the model is numerically consistent and has an acceptable mesh.

Application to Thermal Mechanical Behavior of Continuous-Cast Billet

The finite-element thermal-mechanical model is next applied to predict temperature, bulging, strain, stress and hot tearing in continuous cast steel billets, in the absence of sub-mould support. The results are then used to find the critical casting speeds to avoid quality problems related to bulging below the mold.

Modeling Domain

The model domain is the L-shaped region of one quarter of a transverse section through the billet shown in Fig. 4. Assuming two-fold symmetry and removing the center portion of the section, which is always liquid, saves computational cost.

Heat Flux at Shell Surface

The instantaneous heat flux, given in Eq. 7, is based on fitting many plant measurements of total mold heat flux and differentiating [19]. It is assumed to be uniform around the perimeter of the billet surface in order to simulate ideal taper and perfect contact between the shell and mold. After the billet leaves the mold, its surface temperature is kept unchanged from its circumferential profile at mold exit. This eliminates the effect of spray cooling practice on sub-mold reheating or cooling and the associated complication for the stress/strain development. Transformation temperatures defining the phase evolution of the typical plain carbon steel studied here are given in Table I.

$$q\left(MW/m^2\right)=\begin{cases}5-0.2444t\left(\sec.\right) & t\le 1.0\sec.\\ 4.7556t\left(\sec.\right)^{-0.504} & t>1.0\sec.\end{cases} \tag{7}$$

Simulation Results

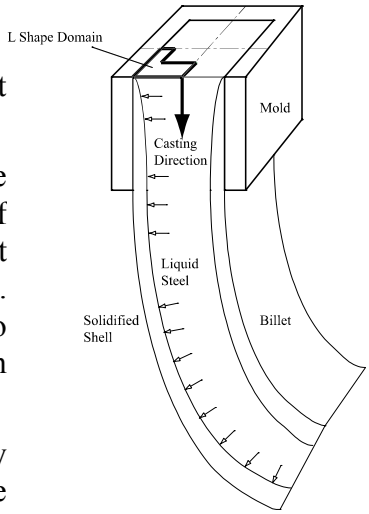

Figure 4: Model Domain

CON2D is used to simulate the mechanical behavior of a steel billet under the conditions shown in Table II with various casting speeds.

Figs. 5(a) and 6(a) show the distorted temperature contours near the strand corner at 200mm below the mold exit for casting speeds of 2.2m/min and 5.0m/min. The latter speed is the critical speed at which hot-tear crack failure of the shell is just predicted to occur. The shell is hotter and thinner at the higher casting speed, owing to less time in the mold. This thinner, hotter, and weaker shell then bulges more under the ferrostatic pressure below the mold.

Figs. 5(b) and 6(b) show contours of "hoop" stress constructed by taking components in the x direction across the dendrites in the horizontal portion of the domain and the y direction in the vertical portion. High values appear at the off-corner sub-surface region, due to a hinging effect that the ferrostatic pressure over the entire face exerts around the corner. This bends the shell around the corner and generates high subsurface tensile stress at the weak solidification front in the off-corner subsurface location. This tensile stress peak increases slightly and moves towards the surface at higher casting speed. Stress concentration is less and the surface hoop stress is compressive at the lower casting speed. This indicates no possibility of surface cracking. However, tensile surface hoop stress is generated below the mold at high speed in Fig. 6(b) at the face center due to excessive bulging. This tensile stress, and the accompanying hot-tear strain, might contribute to longitudinal cracks which penetrate the surface.

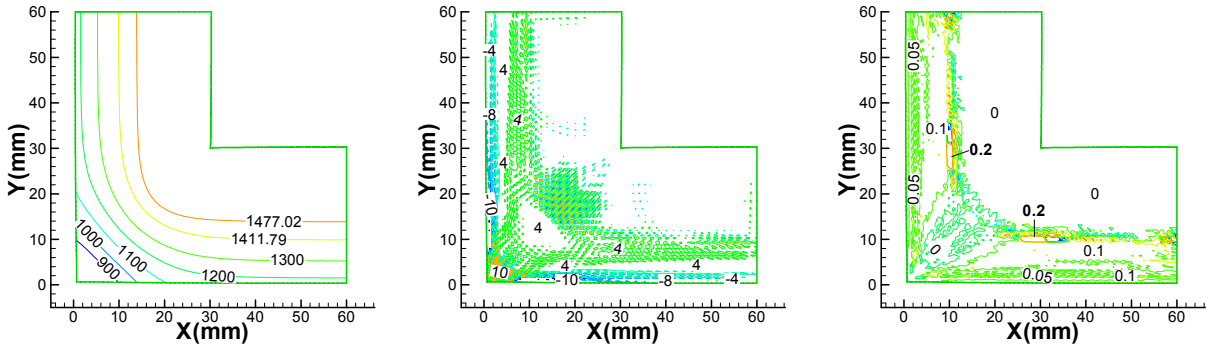

(a) Temperature (b) Hoop Stress (c) Hot-tear Strain

Figure 5: Distorted Contours at 200mm below Mold Exit for the Casting Speed of **2.2m/min**

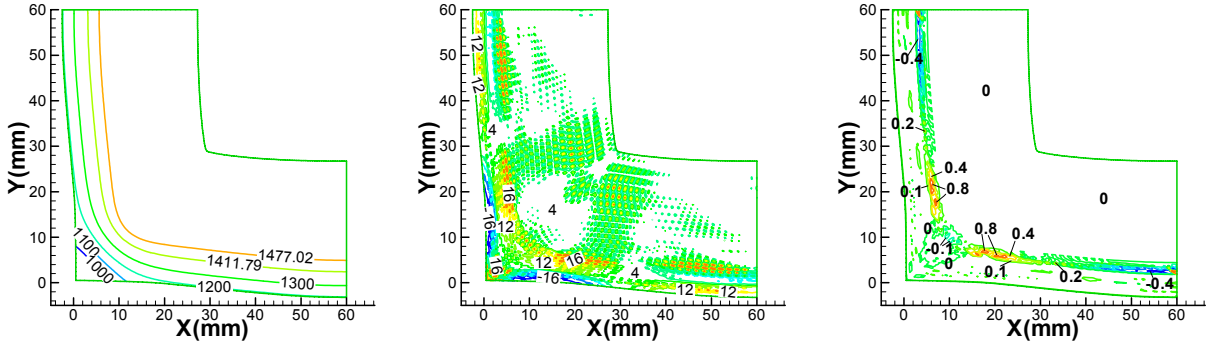

(a) Temperature (b) Hoop Stress (c) Hot-tear Strain

Figure 6: Distorted Contours at 200mm below Mold Exit for the Casting Speed of **5.0m/min**

Figs. 5(c) and 6(c) show contours of hot-tear strain accumulated according to Eq. 6. The highest values of hot-tear strain appear at the off-corner sub-surface region in the hoop direction. Moreover, significantly higher values are found for the higher casting speed. The hot-tear strain in the hoop direction exceeds the threshold at 12 nodes, all located near the off-corner subsurface region at 5.0 m/min. This is caused by the hinging mechanism around the corner. No nodes fail at 2.2m/min or at the center surface. The effect of mold length and section size on the critical casting speed is discussed elsewhere [19]. The critical casting speed predictions match industrial experience [20].

The predicted hot-tearing region matches the location of off-corner longitudinal cracks observed in sections through the solidifying shell, such as pictured in Fig. 7. The bulged shape is also similar. Results from many computations determined the critical speed to avoid cracks as a function of section size and working mold length, presented in Fig. 8. These predictions slightly exceed plant practice, which is generally chosen by empirical trial and error. This suggests that plant conditions such as mold taper are less than ideal, that other factors limit casting speed, or those speeds in practice could be increased. The qualitative trends are the same. Larger section sizes are more susceptible to bending around the corner, so have a lower critical speed, resulting in less productivity increase than expected. The trend towards longer molds over the past 3 decades enables a higher casting speed without cracks by producing a thicker, stronger shell at mold exit.

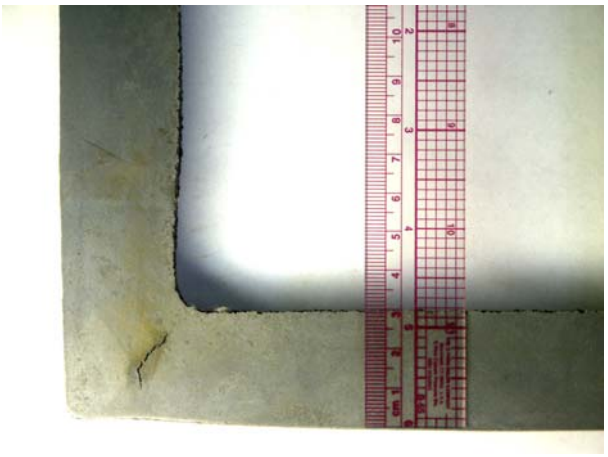

Figure 7: Off-corner internal crack in a 175 mm square bloom

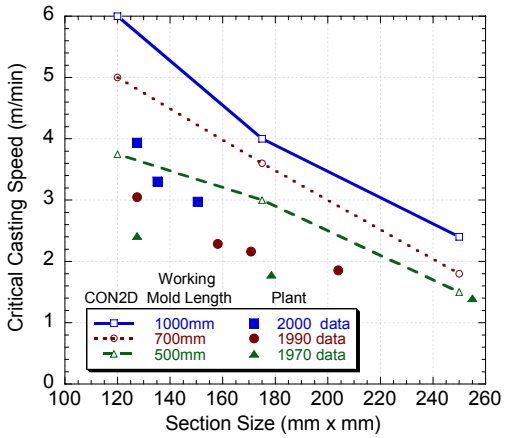

Figure 8: Comparison of critical casting speeds, based on hot-tearing criterion, and typical plant practice [20]

Conclusions

A thermal-mechanical finite-element model, CON2D, has been developed to analyze the thermal-mechanical behavior of the solidifying shell in the continuous casting of steel. This is a Lagrangian approach with a 2-D generalized plane strain condition featuring unified elastic-viscoplastic constitutive models for solid phases, an elastic-perfect-plastic constitutive model for liquid, and a robust and efficient time integration technique. An empirical hot-tear failure criterion is used to predict hot tear cracks quantitatively. This model is then applied to investigate the effect of casting speed during continuous casting of a square steel billet. If casting speed exceeds a critical threshold, then sub-surface, off-corner longitudinal hot-tear cracks are predicted to form due to sub-mold bulging causing tensile bending strain in the off-corner subsurface. The critical casting speeds to avoid those hot tears vary from only 1.5 m/min for short (600 mm length) and large sections (250 mm) to 6.0 m/min for long (1100 mm length) and small sections (120 mm).

References

1. J. K. Brimacombe, "Design of continuous casting machines based on a heat-flow analysis: state-of-the-art review", *Canadian Metall. Quarterly*, 15, (2) (1976), 163-175.
2. J. O. Kristiansson, "Thermal Stresses in the Early Stage of Solidification of Steel", *J. Therm. Stresses*, 5, (3-4) (1982), 315-330.
3. J. E. Kelly, K. P. Michalek, T. G. O'Connor, B. G. Thomas and J. A. Dantzig, "Initial Development of Thermal and Stress Fields in Continuously Cast Steel Billets", *Metall. Trans. A*, 19A, (10) (1988), 2589-2602.
4. A. E. Huespe, A. Cardona and V. Fachinotti, "Thermomechanical model of a continuous casting process", *Computer Methods in Appl. Mech. & Engr.*, 182, (3) (2000), 439-455.
5. A. Moitra, "Thermo-Mechanical Model of Steel Shell Behavior in Continuous Slab Casting" (Ph.D. Thesis, UIUC, 1993), 217.
6. H. Zhu, "Coupled Thermal-Mechanical Finite-Element Model with Application to Initial Solidification" (Ph.D. Thesis, UIUC, 1996), 132.
7. J.-C. T. Parkman, "Simulation of Thermal Mechanical Behavior During Initial Solidification of Steel" (Master Thesis, UIUC, 2000), 139.
8. E. Lemmon, "Multi-dimentional Integral Phase Change Approximations for Finite-Element Conduction Codes", *Numerical Methods in Heat Transfer,* ed. R. W. Lewis, K. Morgan and O. C. Zienkiewicz John Wiley & Sons, 1981), 201-213.
9. T. Dupont, G. Fairweather and J. P. Johnson, "Three-Level Galerkin Methods for Parabolic Equations", *SIAM Journal on Numerical Analysis*, 11, (2) (1974), 392-410.
10. P. F. Kozlowski, B. G. Thomas, J. A. Azzi and H. Wang, "Simple Constitutive Equations for Steel at High Temperature", *Metall. Trans. A*, 23, (March) (1992), 903-918.
11. P. J. Wray, "Effect of Crabon Content on the Plastic Flow of Plain Carbon Steels at Elevated Temperatures", *Metall. Trans. A*, 13A, (January) (1982), 125-134.
12. T. Suzuki, K. H. Tacke, K. Wunnenberg and K. Schwerdtfeger, "Creep Properties of Steel at Continuous Casting Temperatures", *Ironmaking and Steelmaking*, 15, (2) (1988), 90-100.
13. B. G. Thomas and J. T. Parkman, "Simulation of Thermal Mechanical Behaviour During Initial Solidification" (Paper presented at the Thermec '97 Intl. Conf. on Thermomechanical Proc. of Steel and Other Materials, Wollongong, Australia, July 7-11, 1997), II.
14. P. J. Wray, "Plastic Deformation of Delta-Ferritic Iron at Intermediate Strain Rates", *Metall. Trans. A*, 7A, (November) (1976), 1621-1627.
15. J. Lemaitre and J. L. Chaboche, *Mechanics of Solid Materials* (New York, NY: Cambridge University Press, 1990), 556.
16. A. M. Lush, G. Weber and L. Anand, "An Implicit Time-Integration Procedure for a Set of Integral Variable Constitutive Equations for Isotropic Elasto-Viscoplasticity", *International Journal of Plasticity*, 5, (1989), 521-549.
17. Y. Won, T.-J. Yeo, D. Seol and K. Oh, "A New Criterion for Internal Crack Formation in Continuously Cast Steels", *Metall. Trans. B*, 31B, (4) (2000), 779~794.
18. J. H. Weiner and B. A. Boley, "Elasto-Plastic Thermal Stresses in A Solidifying Body", *J. Mech. Phys. Solids*, 11, (1963), 145-154.
19. C. Li and B. G. Thomas, "Maximum Casting Speed for CC Steel Billets Based on Sub-mold Bulging Computation" (Paper presented at the 85th Steelmaking Conf., Nashiville, TN, Mar. 11~13, 2002), 85.
20. E. Howard and D. Lorento, "Development of High Speed Casting" (Paper presented at the 1996 Electric Furnace Conference Proceedings, Dallas, TX, Dec. 9~12, 1996),

Acknowledgements

The authors thank the steel industry members of the Continuous Casting Consortium for their financial support of this project and the National Center for Supercomputing Applications at UIUC for computing time. Work by previous students, A. Moitra, H. Zhu, and J. Parkman, on the CON2D program is also gratefully acknowledged.